

Formulation and validation of a quasi-static Material Point Method

L. Beuth, T. Benz & P.A. Vermeer
University of Stuttgart, Germany

C.J. Coetzee
University of Stellenbosch, South Africa

P. Bonnier
PLAXIS B.V., Delft, the Netherlands

P. van den Berg
GeoDelft, Delft, the Netherlands

ABSTRACT: The Finite Element Method (FEM) has become the standard tool for the analysis of a wide range of solid mechanics problems. However, the underlying structure of a classical updated Lagrangian FEM is not well suited for the treatment of large deformation problems, since excessive mesh distortions can lead to numerical difficulties. The Material Point Method (MPM) represents an approach in which material points moving through a fixed finite element grid are used to simulate large deformations. As the method makes use of moving material points, it can also be classified as a point-based or meshless method. With no mesh distortions, it is an ideal tool for the analysis of large deformation problems. MPM has its origin in fluid mechanics and has only recently been applied to solid mechanics problems. It has been used successfully for impact analyses where bodies penetrate each other and for silo discharging problems. All existing MPM codes found in literature are dynamic codes with explicit time integration and only recently implicit time integration. In this study a quasi-static MPM formulation and implementation are presented. The paper starts with the description of the quasi-static governing equations and the numerical discretisation. Afterwards, the calculation process of the quasi-static MPM is explained, followed by the presentation of benchmark problems which have been calculated with the newly developed quasi-static MPM code. The benchmark problems consist of the oedometer test and large elastic bending of a cantilever beam. For validation, the results are compared with analytical solutions and FEM results.

1 INTRODUCTION

Over the last 25 years, the Finite Element Method (FEM) has become a standard tool for the analysis of a wide range of solid mechanics problems. However, FEM is not well suited for the modelling of large deformation problems. When these problems are modelled with an updated Lagrangian finite element method, considerable mesh distortions occur, which require remeshing. During the remeshing process all the state variables have to be mapped from the distorted mesh to the newly defined mesh, which introduces errors (Więckowski, 2001).

To overcome the difficulties of FEM, so-called meshless methods have been developed, for example the Element-Free Galerkin Method and Smoothed Particle Hydrodynamics (Li, 2002). The Material Point Method (MPM) might be classified as a meshless method, a particle method or an Arbitrary Lagrangian-Eulerian (ALE) method (Więckowski, 1999).

MPM uses two discretizations of the material, one based on a computational mesh and the other based on a collection of material points or “particles”. All the properties of the continuum (material

data and deformation state) as well as the external loads are carried by the material points, while the grid carries no permanent information. The computational grid is used to determine incremental displacements by solving the governing equations as with the standard finite element method. With the MPM large deformations are modelled by moving material points through the mesh. By this approach, MPM combines the advantages of both Eulerian and Lagrangian formulations.

The early beginnings of MPM can be traced back to the work of Harlow (1964), who studied fluid flow by material points moving through a fixed grid. Sulsky *et al.* (1995) later extended the approach for the modelling of solid mechanics and called it the Material Point Method. Bardenhagen *et al.* (2000) extended the method further to include frictional contact between deformable solid bodies.

The potential of MPM for simulating granular flow was first recognised by Więckowski (1998). Several papers on MPM modelling of silo discharge were published (Więckowski, 1999, 2001, 2003). Coetzee (2004) and Coetzee *et al.* (2005) extended the method to include a micro-polar Cosserat con-

tinuum for studying anchor pull-out and the large deformation problem of excavator bucket filling.

Most MPM implementations developed so far are dynamic codes which employ an explicit time integration scheme. Although it is possible to use these programs also for the analysis of quasi-static problems, this is computationally inefficient as explicit integration requires very small time steps and can lead to long computation times. For these reasons, it was decided to develop a quasi-static MPM implementation which uses an implicit integration scheme, thereby broadening the possibilities of large deformation analyses for complex, large-scale geotechnical problems.

MPM is based on FEM so that many of the standard FEM routines can be used. The MPM code presented in this paper is based on an existing updated Lagrangian FEM code (Plaxis, 2006).

2 QUASI-STATIC MPM FORMULATION

In this section the field equations of quasi-static large deformation are presented. It is followed by a description of the numerical discretisation and integration.

2.1 Field equations of quasi-static deformation

The internal static equilibrium of a continuum can be written as

$$\frac{\partial \sigma_{ij}}{\partial x_j} + \gamma_i = 0 \quad (1)$$

and on the external boundary S as

$$\tau_i = \sigma_{ij} \cdot n_j \quad i,j,k = 1,2,3 \quad (2)$$

where x_j are Cartesian coordinates, σ_{ij} denotes the Cauchy stress tensor, γ_i represents body forces and τ_i denotes the boundary traction components.

Applying Galerkin's variational principle followed by integration by parts (Green's theorem) yields the equilibrium equation in the weak form

$$\int_V \sigma_{ij} \cdot \frac{\partial \delta u_i}{\partial x_j} dV = \int_V \gamma_i \cdot \delta u_i dV + \int_S \tau_i \cdot \delta u_i dS \quad (3)$$

where δu_i represents a kinematically admissible variation of displacements, i.e. a virtual displacement.

The development of the stress state σ_{ij} can be regarded as an incremental process

$$\sigma_{ij} = \sigma_{ij}^0 + \Delta \sigma_{ij} \quad (4)$$

In this relation σ_{ij} represents the actual state of stress at the end of a load step and σ_{ij}^0 represents the pre-

vious state of stress at the beginning of this particular load step. Equation 3 can now be written as

$$\int_V \Delta \sigma_{ij} \cdot \frac{\partial \delta u_i}{\partial x_j} dV = \int_V \gamma_i \cdot \delta u_i dV + \int_S \tau_i \cdot \delta u_i dS - \int_V \sigma_{ij}^0 \cdot \frac{\partial \delta u_i}{\partial x_j} dV \quad (5)$$

So far, the final configuration for x_i and V is taken as a reference configuration. However, at the beginning of an increment, this configuration is not known. Therefore, Equation 5 is reformulated so that the variables of the initial geometry x_i^0 and V^0 of a load step are used as the reference configuration

$$\int_{V_0} \Delta \Sigma_{ji} \cdot \frac{\partial \delta u_i}{\partial x_j^0} dV_0 = \int_{V_0} \gamma_i \cdot \delta u_i dV_0 + \int_{S_0} \tau_i \cdot \delta u_i dS_0 - \int_{V_0} \sigma_{ij}^0 \cdot \frac{\partial \delta u_i}{\partial x_j^0} dV_0 + \text{Higher Order Terms} \quad (6)$$

where Σ_{ji} is the first Piola-Kirchhoff stress tensor. The increment of the first Piola-Kirchhoff stress tensor can be written as

$$\Delta \Sigma_{ji} = \Delta \sigma_{ji} - \sigma_{ki}^0 \cdot \frac{\partial \Delta u_j}{\partial x_k^0} + \sigma_{ji}^0 \cdot \frac{\partial \Delta u_k}{\partial x_k^0} \quad (7)$$

Due to the second term, this stress rate is non-symmetric. The Cauchy stress increment $\Delta \sigma_{ij}$ can be written as:

$$\Delta \sigma_{ij} = \Delta \sigma_{ij}^J + \sigma_{ik}^0 \cdot \Delta \omega_{kj} + \sigma_{jk}^0 \cdot \Delta \omega_{ki} \quad (8)$$

where $\Delta \sigma_{ij}^J$ is the Jaumann stress rate. The incremental strains $\Delta \varepsilon_{ij}$ and rotations $\Delta \omega_{ij}$ are given by

$$\Delta \varepsilon_{ij} = \frac{1}{2} \left(\frac{\partial \Delta u_i}{\partial x_j^0} + \frac{\partial \Delta u_j}{\partial x_i^0} \right) \quad (9)$$

$$\Delta \omega_{ij} = \frac{1}{2} \left(\frac{\partial \Delta u_j}{\partial x_i^0} - \frac{\partial \Delta u_i}{\partial x_j^0} \right) \quad (10)$$

The constitutive relation between the Jaumann stress increment and the strain increment is

$$\Delta \sigma_{ij}^J = D_{ijkl} \cdot \Delta \varepsilon_{kl} - \sigma_{ij}^0 \cdot \Delta \varepsilon_{kk} \quad (11)$$

where D_{ijkl} is the elastic element stiffness matrix.

The left hand side of Equation 6 now becomes

$$\int_{V_0} D_{ijkl}^0 \cdot \Delta \varepsilon_{kl} \cdot \delta \varepsilon_{ij} dV_0 + \int_{V_0} \left[\sigma_{ki}^0 \cdot \Delta u_{j,k} \cdot \delta u_{j,i} - 2 \cdot \sigma_{ki}^0 \cdot \Delta \varepsilon_{jk} \cdot \delta \varepsilon_{ij} \right] dV_0 = \text{Right Hand Side} \quad (12)$$

where the first term is the usual (small strain) internal virtual work and the second term contains the large deformation contribution (van Langen, 1991).

2.2 Numerical discretisation and integration

The element mesh used in MPM is identical to a FEM mesh. Interpolation functions are used to interpolate nodal values to the interior of an isoparametric element. Making use of matrix notation, the displacement field $\underline{\Delta u}$, for example, is given by

$$\underline{\Delta u} = \underline{N}(\xi, \eta, \zeta) \cdot \underline{\Delta v} \quad (13)$$

where $\underline{\Delta v}$ is the nodal displacement vector, \underline{N} is assembled from shape functions and ξ, η and ζ are the local coordinates respectively.

The strains at any point within the finite elements are determined from the nodal displacements $\underline{\Delta v}$

$$\underline{\Delta \varepsilon} = \underline{L} \cdot \underline{\Delta u} = \underline{L} \cdot \underline{N} \cdot \underline{\Delta v} = \underline{B} \cdot \underline{\Delta v} \quad (14)$$

where \underline{L} contains the Cartesian differential operators and \underline{B} denotes the well-known strain interpolation matrix.

Making use of these definitions, the equilibrium equation, given by Equation 12, now becomes

$$\left[\underline{K}^E + \underline{K}^G \right] \cdot \underline{\Delta v} = \underline{f}_{\text{load}} - \underline{f}_{\text{internal}} + \text{Higher Order Terms} \quad (15)$$

where the elastic stiffness matrix is given by

$$\underline{K}^E = \int_{V_0} \underline{B}^T \cdot \underline{D} \cdot \underline{B} \, dV_0 \quad (16)$$

and the geometric stiffness matrix is determined from the stresses $\underline{\sigma}^0$ at the beginning of the load step

$$\underline{K}_{qp}^G = \int_{V_0} \left[L_{jpk} \cdot \sigma_{ki}^0 \cdot L_{jqk} - 2 \cdot B_{jpk} \cdot \sigma_{ki}^0 \cdot B_{iqj} \right] dV_0 \quad (17)$$

$$\text{with } L_{ijk} = N_{ij,k} \text{ and } B_{ijk} = \frac{1}{2} \cdot [L_{ijk} + L_{kji}] \quad (18)$$

The external load vector contains body forces and surface tractions

$$\begin{aligned} \underline{f}_{\text{load}} &= \underline{f}_{\text{body}} + \underline{f}_{\text{traction}} \\ &= \int_{V_0} \underline{N}^T \cdot \underline{\gamma} \, dV_0 + \int_{S_0} \underline{N}^T \cdot \underline{\tau} \, dS_0 \end{aligned} \quad (19)$$

while the internal (reaction) force vector is given by

$$\underline{f}_{\text{internal}} = \int_{V_0} \underline{B}^T \cdot \underline{\sigma} \, dV_0 \quad (20)$$

Because of the higher-order terms on the right hand side, Equation 15 has to be solved iteratively as described in the following section.

In standard FEM, Gauss-Legendre integration is used to integrate the stiffness terms over the element volume with a fixed number of integration points. In MPM, the integration is performed over the (changing) volume Ω_p of the element's material points. The elastic and geometric element stiffness matrices given by Equation 16 and 17 are then respectively given by

$$\underline{K}^E = \sum_{p=1}^{n_p} \underline{B}^T \cdot \underline{D} \cdot \underline{B} \cdot \Omega_p \quad (21)$$

and

$$\underline{K}_{qm}^G = \sum_{p=1}^{n_p} \left[L_{jmk} \cdot \sigma_{ki}^0 \cdot L_{jqk} - 2 \cdot B_{jmk} \cdot \sigma_{ki}^0 \cdot B_{iqj} \right] \Omega_p \quad (22)$$

where n_p denotes the variable number of material points per element. The components of the external load vector given by Equation 19 are integrated as follows

$$\underline{f}_{\text{body}} = \sum_{p=1}^{n_p} \underline{g} \cdot \underline{N}_p^T \cdot m_p ; \quad \underline{f}_{\text{traction}} = \sum_{p=1}^{n_p} \underline{N}_p^T \cdot \underline{t}_p \quad (23)$$

where m_p is the material mass assigned to the material point, \underline{g} is the gravitational acceleration vector and \underline{t}_p the traction force applied on a particle. The internal force vector (Equation 20) is integrated in a similar way

$$\underline{f}_{\text{internal}} = \sum_{p=1}^{n_p} \underline{B}^T \cdot \underline{\sigma}_p \cdot \Omega_p \quad (24)$$

3 MPM CALCULATION PROCESS

In MPM, a set of material points is tracked throughout the deformation history of a body. The full numerical solution is calculated at these material points. Global position, stress and strain, for example, are associated with these material points.

The calculation process of the quasi-static MPM can be divided into three steps:

During the *Initialisation Phase*, the initial values of quantities assigned to material points are set from initial data defining the given problem. The information carried by the material points is projected onto a background finite element mesh where equations of motion are solved in an updated Lagrangian frame. Information from this solution is then used to update the material points.

The solution on the mesh is called the *Lagrangian Phase* of the calculation. Once the material points have been updated, the mesh is reset to its initial configuration. The movement of the mesh relative to the material points models convection, and is

called the *Convective Phase* of the calculation (Sulsky & Schreyer, 1996).

With reference to the equations given in the previous section, each of the MPM calculation phases is described in more detail.

3.1 The Initialisation Phase

This phase starts by generating a finite element mesh. In contrast to FEM, the mesh is not only generated where material exists, but over the complete domain where material is expected to move.

Material points are placed inside elements to form (define) the solid body. This is shown in Figure 1, for the simple case of a cantilever. Elements containing material points are called *activated elements* and elements containing no material points are called *deactivated elements*. As material points move through the grid, elements become activated and deactivated using a special house-keeping algorithm. Similar to FEM, constraints are handled by fixing nodes, i.e. zero displacements are enforced at these nodes (Figure 1).

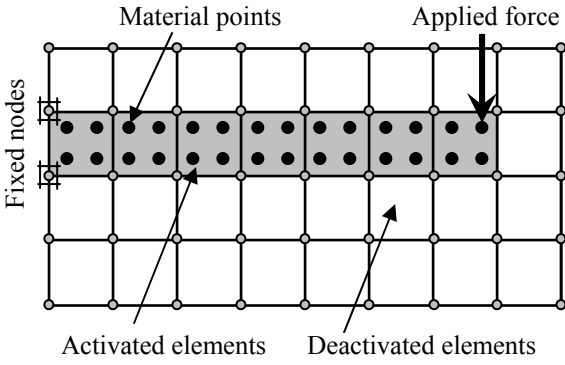


Figure 1. Initialisation Phase.

During the Initialisation Phase, loads are assigned to material points which they carry throughout the deformation process. The material points are initially evenly distributed in an element, and thus each given the same weight.

In the 3D code presented in this paper, 6-noded wedge elements were used with linear shape functions (Plaxis, 2006) and initially 8 material points per element, each with a weight of $w_p = 1/8$.

3.2 The Lagrangian Phase

With all the state variables initialised at material points during the Initialisation Phase, the Lagrangian Phase can be executed. The result of the Lagrangian Phase are nodal displacement increments solved through an iterative procedure. The modified Newton-Raphson procedure can be described as follows:

The first step of the Lagrangian Phase is to calculate the external load vector (Equation 23), the elastic stiffness matrix (Equation 21) and the geometric

stiffness matrix (Equation 22) using the current location of material points within the activated elements.

The formulation of the iterative procedure starts with the linearized equilibrium equation (Equation 15)

$$\left[\underline{\underline{K}}^E + \underline{\underline{K}}^G \right]^0 \cdot \Delta \underline{v} = \underline{f}_{load} - \underline{f}_{internal}^0 \quad (25)$$

The iterative procedure reads

$$\left[\underline{\underline{K}}^E + \underline{\underline{K}}^G \right]^0 \cdot \delta \underline{v}^k = \underline{f}_{load} - \underline{f}_{internal}^{k-1} \quad (26)$$

where $k = 1, 2, \dots, n$ is the iteration number of the load step considered. Sub-displacement increments (sub-increments) $\delta \underline{v}$ are solved and added together to form the nodal displacement increments

$$\Delta \underline{v}^k = \sum_{l=1}^k \delta \underline{v}^l \quad (27)$$

The initial value of $\underline{f}_{internal}^{k-1}$ for $k=1$ is given by

$$\underline{f}_{internal}^0 = \int_V \underline{\underline{B}}^T \underline{\underline{\sigma}}^0 dV \quad (28)$$

with subsequent values of $\underline{f}_{internal}$ computed from

$$\underline{f}_{internal}^k = \int_V \underline{\underline{B}}^T \underline{\underline{\sigma}}^k dV \quad (29)$$

where the stress update is given by

$$\Delta \sigma_{ij} = D_{ijkl} \cdot \Delta \varepsilon_{kl} - \sigma_{ij} \cdot \Delta \varepsilon_{kk} + \sigma_{ik}^0 \cdot \Delta \omega_{kj} + \sigma_{jk}^0 \cdot \Delta \omega_{ki} \quad (30)$$

The number of iterations is stopped as soon as

$$\left\| \underline{f}_{load} - \underline{f}_{internal}^k \right\| \leq \alpha \cdot \left\| \underline{f}_{load} \right\| \quad (31)$$

where α is a specified tolerance, e.g. $\alpha = 0.01$.

3.3 The Convective Phase

At the end of the Lagrangian Phase, the nodal displacements $\Delta \underline{v}$ are known as shown in Figure 2(b). The mesh is now reset to its initial configuration as shown in Figure 2(c), while the material points keep their global position. The house-keeping algorithm now determines which elements should be activated and which should be deactivated.

The material point volumes Ω_p are updated using

$$\Omega_p^i = \omega_p^{i-1} \cdot \frac{|J_p^{i-1}|}{|J_p^0|} \cdot |J_p^i| \quad (32)$$

where J_p is the Jacobian matrix evaluated at the material point position.

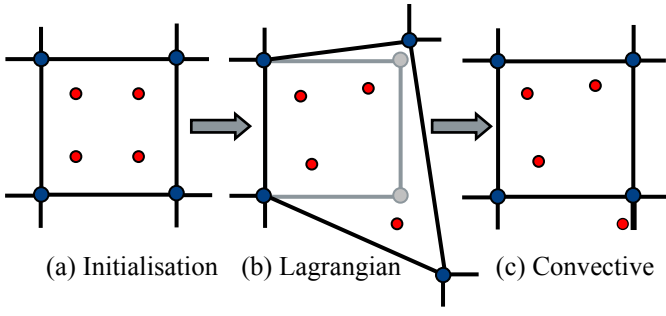


Figure 2. The MPM calculation process: Initialisation Phase, Lagrangian Phase and Convective Phase.

The mass of each material point, used for calculating the body forces (Equation 23), is calculated by

$$m_p = \rho \cdot \Omega_p \quad (33)$$

where ρ is the material density assigned to the material point.

4 RESULTS FOR THE OEDOMETER TEST

The oedometer test provides a one-dimensional deformation problem which can easily be checked for accuracy using an analytical solution.

The analytical solution for the one-dimensional compression of an elastic material is based on the logarithmic strain measure for large deformations (Van Langen, 1991)

$$\varepsilon_L = -\ln\left(\frac{L}{L_0}\right) \quad (34)$$

where ε_L is the logarithmic strain, L_0 the initial height and L is the deformed height of the soil sample in the oedometer. With

$$\frac{L}{L_0} = 1 - \frac{\Delta L}{L_0} = 1 - \varepsilon \quad (35)$$

the formula for the logarithmic strain ε_L can also be written as

$$\varepsilon_L = -\ln(1 - \varepsilon) \quad (36)$$

where ε is the (vertical) engineering strain. For small deformations up to $\varepsilon \approx 0.1$ the logarithmic strain is virtually equal to the engineering strain. Strains above this limit are considered as large deformations.

Van Langen (1991) derived the analytical solution for the Cauchy stress σ as follows: $\sigma = E \cdot [e^{\varepsilon_L} - 1]$. For small values of ε_L this equation simply reduces to $\sigma = E \cdot \varepsilon_L$. The deviation from this linear equation is caused by the fact that Van Langen (1991) assumes a linear relation between the Kirchhoff stress Σ^K and the logarithmic

strain ε_L , i.e. $\Sigma^K = E \cdot \varepsilon_L$, where E is the Young's modulus.

In Figure 3 the stress-strain curves for different mesh refinements are plotted. Up to a logarithmic strain of 0.28 the MPM results correspond well with the analytical solution. Thereafter, a small deviation occurs, with MPM underestimating the oedometer stiffness. The coarse mesh consists of 8 layers of elements (16 elements in total) and the fine mesh of 16 layers (32 elements in total). From the results it can be seen that there is no significant difference in the results from these two meshes.

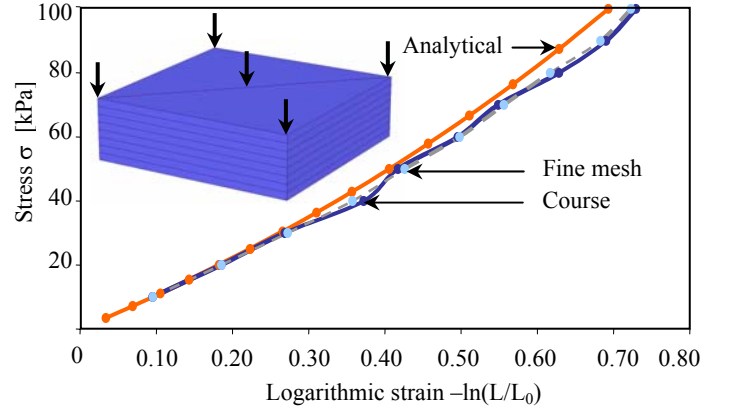


Figure 3. Computed oedometer stress-strain curves for different mesh refinements. 10 load steps, 116 iterations.

5 RESULTS FOR THE CANTILEVER BEAM

The analysed cantilever is shown in Figure 4(a) in its initial configuration. Note that only the activated elements are shown.

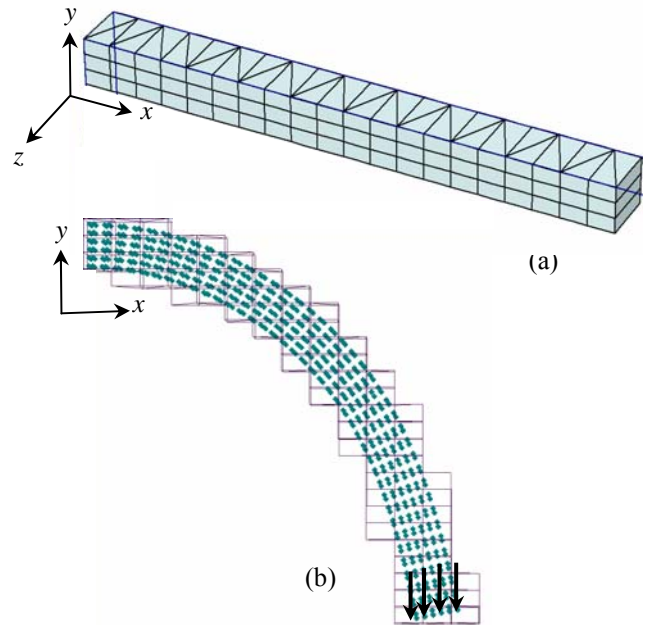


Figure 4. MPM cantilever (a) initial configuration showing the activated elements and (b) the final deformed configuration showing the material points and the activated elements.

The beam has a length of 1.0 m, a height of 0.09 m and a width of 0.1 m. In the initial configuration 120 elements (20x3x2) were used to model the beam. The final deformed configuration is shown in Figure 4(b) where the material points are shown together with the activated elements.

The load-displacement curve calculated with MPM is compared with the results from updated Lagrangian FEM simulations. For the FEM calculations, two element types were used: 15-noded elements with second-order interpolation functions and 6-noded elements with linear interpolation functions (the same elements used for MPM modelling). The load-displacement curves are shown in Figure 5.

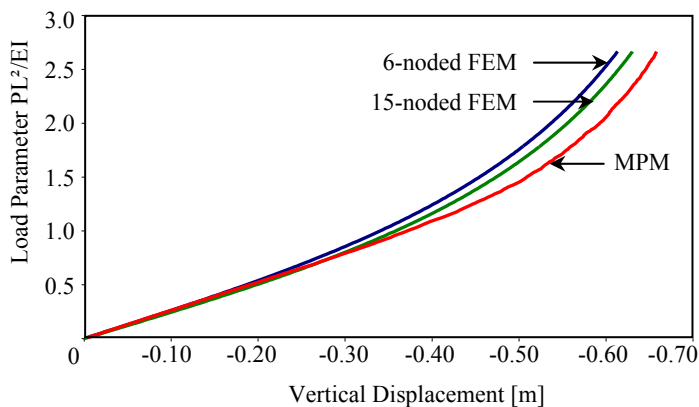


Figure 5. Cantilever load-displacement curves using MPM and FEM.

For the first third of the loading, there is no significant difference between the results from MPM and FEM (both element types). Upon further loading, MPM predicts larger displacements, i.e. underestimates the beam stiffness. The 15-noded FEM analysis also shows larger displacements when compared with 6-noded FEM. It is expected that the higher-order elements model the beam more accurately. In general MPM accurately predicts the beam behaviour although it slightly underestimates the beam stiffness.

6 CONCLUSIONS

The development of a three-dimensional quasi-static MPM code is presented. MPM can model large deformations without the difficulty of mesh distortions and remeshing. The code was implemented using an existing updated Lagrangian FEM code and results from oedometer tests and large deformation cantilever problems compared to analytical models and FEM results.

It is shown that MPM can model the large deformations of an oedometer. During the initial stages of loading, MPM accurately predicts the stress-strain curve. Towards the latter stages of loading, MPM however predicts displacements slightly too large.

It is also shown that MPM can model the large deformation of a cantilever. The load-displacement curve corresponds well with the results from FEM for the first third of the loading process. Thereafter, MPM predicts displacements slightly too large.

In both the oedometer and the cantilever problems, MPM underestimates the stiffness of the body especially towards the latter stages of loading. It is believed that better results can be achieved if more material points per element are used. Results should also be more accurate if higher-order elements are used.

In the current MPM implementation 6-noded wedge elements with linear interpolation functions are used. In the future, 15-noded wedge elements with second-order interpolation functions will be implemented. In this paper the material was assumed to be elastic, in the future plasticity will be added.

It is concluded that MPM is well suited for the modelling of large deformation problems. Geotechnical applications such as pile driving, installation of spudcans and bucket foundations will be investigated in the near future.

7 REFERENCES

- Bardenhagen, S.G. Brackbill, J.U. & Sulsky, D. 2000. The material-point method for granular materials. *Computational Methods in Applied Mechanics and Engineering* 187: 529–541.
- Coetzee, C.J. 2004. *The modelling of granular flow using the particle-in-cell method*. PhD Thesis, Department of Mechanical Engineering, University of Stellenbosch, South Africa.
- Coetzee, C.J. Vermeer, P.A. & Basson, A.H. 2005. The modelling of anchors using the material point method. *International Journal for Numerical and Analytical Methods in Geomechanics* 29: 879-895.
- Harlow, F.H. 1964. The particle-in-cell computing method in fluid dynamics. *Methods in Computational Physics*. 3: 319-343.
- Li, S. & Liu, W.K. 2002. Meshfree and particle methods and their applications. *Appl. Mech. Rev.* 55(1).
- Plaxis B.V. 2006. *Plaxis 3D Foundation Scientific Manual*. Version 1.5.
- Sulsky, D. & Schreyer, H.L. 1996. Axisymmetric form of the material point method with applications to upsetting and Taylor impact problems. *Comput. Methods Appl. Mech. Engrg.* 139: 409-429.
- Van Langen, H. 1991. *Numerical Analysis of Soil-Structure Interaction*. PhD Thesis, Faculty of Civil Engineering, Delft University of Technology.
- Więckowski, Z. 1998. A particle-in-cell method in analysis of motion of a granular material in a silo. *Computational Mechanics: New trends and Applications*.
- Więckowski, A. 1999. A particle-in-cell solution to the silo discharging problem. *Int. J. Numer. Meth. Engrng* 45: 1203-1225.
- Więckowski, Z. 2001. Analysis of granular flow by the material point method. In European Conference on Computational Mechanics, June 26-29, Cracow, Poland.
- Więckowski, Z. 2003. Modelling of silo discharge and filling problems by the material point method. *Task Quarterly* 4: 701–721, 2003.